

Chapter 4

Effect of 120 MeV Ni¹⁰⁺ ions Irradiation on Ni-DMG Dispersed PMMA Films

Abstract

In this chapter effects of 120 MeV, Ni¹⁰⁺ ions were studied on Nickel dimethylglyoxime (Ni-DMG) dispersed PMMA films at different fluences. The results obtained from different characterization techniques showing the fluence dependent modification of above polymer composite and discussed in terms of electrical properties, Vickers hardness, particle size and crystallinity and surface morphology. These properties were discussed in terms of ion fluence and concentration of filler.

4.0 Introduction

Swift heavy ion (SHI) irradiations play a very significant role for the modification of the properties of materials. The effect of ion beam on materials depends on the ion energy, fluence and ion species [1, 2]. The ions loss energy during their passage through the material either by exciting the atoms due to inelastic collision which is characterized by the electronic stopping power or by displacing the atoms due to elastic collision, which is characterized by the nuclear stopping power. It has been shown that defects created by the nuclear energy loss can be used as nucleation sites for the formation of nanoparticles and nanoparticles grow without thermal annealing during low energy ion irradiation [3]. Valentine et al. [4] demonstrated that the nucleation of nano clusters can take place if electronic stopping power (S_e) exceeds a certain threshold value and the clusters grow via Ostwald ripening during post irradiation annealing. The cluster density has been shown to correlate with S_e and nanoclusters with quite narrow size distribution have been produced [4]. Since irradiation generally creates defects states in the material, it has been and being used to control the material properties. It is well known that a large fraction of point defects, created in material by energetic particle irradiation, recombine spontaneously. At elevated temperatures, the motion of the remaining defects (1-2%) leads to radiation enhanced diffusion and formation of defect clusters and dislocation loops in conventional materials [5, 6]. Alternately, point defects can also annihilate at grain boundaries.

However, the appearance of track effects in polymers is known from some decades [7], there is hardly any report on SHI modification of dielectric properties and semi-crystalline structure of chemically synthesized polymer embedded metal compound

composites. The fabrication of such composites is relatively cheaper and a simpler chemicals route is useful for large scale productions. In addition, such chemically process system where nanoparticles are embedded in to a polymer matrix are important due to the suppression of grain boundary problem, hence upon irradiation by SHI with high electronic energy loss, one would extract information of individual nanoparticles than that of an assembly and macroscopic modifications of polymer composite films.

In this work, different concentrations of nickel dimethylglyoxime (Ni-DMG) compound dispersed polymethyl methacrylate (PMMA) films were irradiated with high energy ions and modifications in dielectric property, crystalline structures and microhardness are followed by means of LCR meter, X-ray diffraction (XRD) measurements and Vickers' microhardness indentation. The surface topography was also studied by AFM and SEM. Sample preparation and irradiation details have been discussed in article 2.3.1 of Chapter 2. The samples were irradiated with 120 MeV Ni¹⁰⁺ ions and characterized by different techniques as discussed in article 2.4 of Chapter 2 [8, 9].

4.1 Results and Discussion

4.1.1 AC Electrical Frequency Response

4.1.1 (a) Conductivity vs frequency

AC electrical measurement was performed for pristine and irradiated samples. Fig.4.1 (a, b and c) shows the variation of conductivity with frequency for the pristine and irradiated samples at different ferric oxalate concentration. The conductivity was calculated using equation 2.5 as discussed in article 2.4.1 of Chapter 2.

A sharp increase in conductivity was observed in pristine as well as irradiated samples. It was also observed that conductivity increases with increasing concentration of dispersed Ni-DMG compound (Fig.4.1a, pristine) as well as those irradiated at the fluence of 1×10^{11} ions/cm² (Fig.4.1b) and 1×10^{12} ions/cm² (Fig.4.1c) respectively. The increase in conductivity with different Ni-DMG concentration for pristine samples may be attributed to the conductive phase formed by dispersed organometallic compound in polymer matrix. It is known that electrical conductivity of such composites depends on the type and concentration of the dispersed compound [10, 11]. As a result the conductivity of dispersed films increases with increasing the concentration of ferric oxalate compound in the polymer matrix. It is also observed that after the irradiation the conductivity increases with fluence (Fig.4.1). Irradiation is expected to promote the metal to polymer bonding and convert the polymeric structure in to hydrogen depleted carbon network. It is this carbon network that is believed to make the polymers more conductive [12].

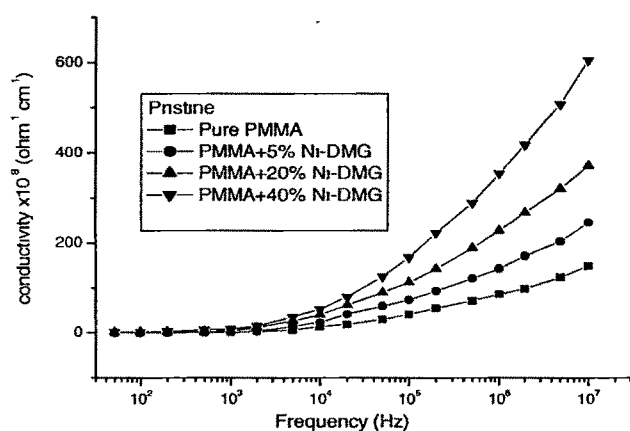


Figure 4.1(a) AC conductivity versus frequency for pristine pure and dispersed Ni DMG in PMMA films.

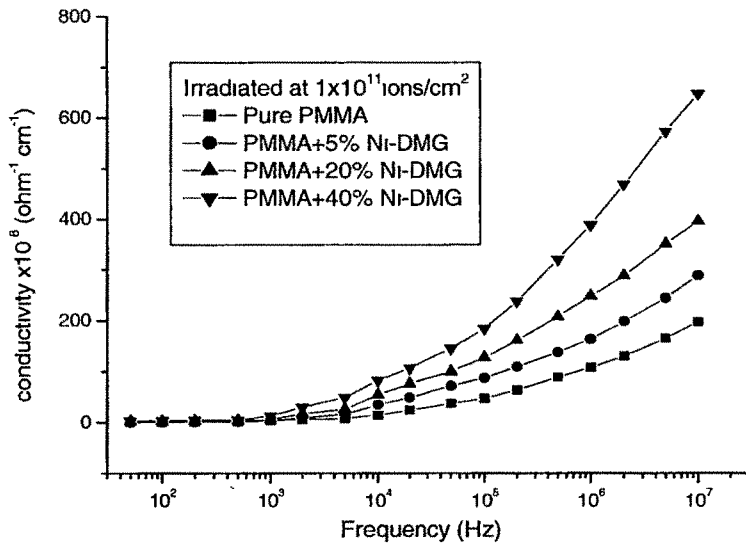


Figure 4.1(b) AC conductivity versus frequency for irradiated (at the fluence of 1×10^{11} ions/cm²) pure and dispersed Ni-DMG in PMMA films.

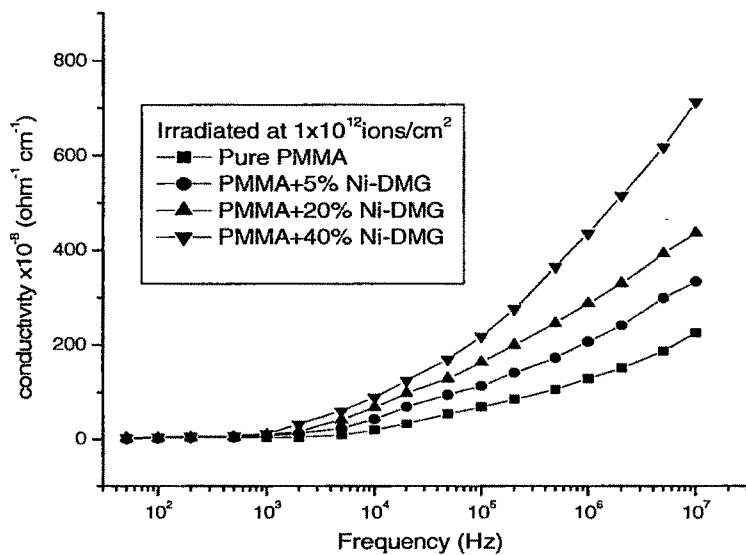


Figure 4.1(c) AC conductivity versus frequency for irradiated (at the fluence of 1×10^{12} ions/cm²) pure and dispersed Ni-DMG in PMMA films.

4.1.1 (b) Dielectric constant vs frequency

The dielectric constant was calculated using formula 2.8 as discussed in article 2.4 1 of Chapter 2. The dielectric constant is studied with respect to the frequency at different concentration of Ni-DMG for pristine and irradiated samples.

Fig 4.2 (a, b and c) shows the plot of dielectric constant versus frequency for pristine and irradiated samples of pure PMMA and different concentration of Ni-DMG dispersed PMMA films. When the fillers are dispersed in the insulating polymer, the dielectric constant of composites investigated increases with concentration of fillers. Such results have been observed experimentally [13, 14]. The partial agglomerations also increases with increasing the filler concentration as shown in Fig 4.10 (AFM).

As evident from Fig 4.2, the dielectric constant remains almost constant up to 100 kHz. At these frequencies, the motion of the free charge carriers is constant and so the dielectric constant presumably remains unchanged. It is also observed that dielectric constant increases for irradiated films with fluence. The increase in dielectric constant may be attributed to the chain scission and as a result the increase in the number of free radicals, etc. As frequency increases further (i.e. beyond 100 kHz), the charge carriers migrate through the dielectric and get trapped against a defect sites and induced an opposite charge in its vicinity. At these frequencies, the polarization of trapped and bound charges can not take place and hence the dielectric constant decreases [15]. The dielectric constant decreases at higher frequencies (i.e. beyond 100 kHz) obeys the Universal law [15, 16] of dielectric response given by $\epsilon \propto f^{-n}$, where n is power law exponent and varies form zero to one ($0 < n < 1$), $n=0.76$ for pure PMMA, 0.63 for 5%, 20% and 40% Ni-DMG dispersed pristine films were observed respectively. The value of

$n=0.97$ and 0.82 for pure PMMA; 0.80 and 0.74 for 5%, 0.69 and 0.74 for 20% and 0.69 and 0.74 for 40% dispersed Ni-DMG dispersed irradiated samples were obtained at the fluence of 1×10^{11} ions/cm² (Fig. 4.2b) and 1×10^{12} ions/cm² (Fig 4.2c) respectively.

The Fig. 4.2 (a, b and c) clearly shows that the frequency dependence of dielectric constant, ϵ , obeys Universal law. The observed nature of the fluence dependence of dielectric constant in studied frequency range can be explained by the prevailing influence of the enhanced free carriers due to the irradiation [17].

4.1.1 (c) Dielectric loss vs frequency

The dielectric loss is studied with respect to frequency at different concentration of Ni-DMG for pristine and irradiated samples. Fig.4.3 (a, b and c) shows the variation of dielectric loss with log frequency for pristine and irradiated samples of pure PMMA and Ni-DMG dispersed PMMA films at the concentration of 5%, 20% and 40% respectively. The dielectric loss decreases with increasing frequency. It is noticed that dielectric loss increases on increasing the concentration of filler and also with the fluence. The increase in $\tan\delta$ as the increase in conductivity is brought about by an increase in the conduction of residual current and the conduction of absorbance current [18].

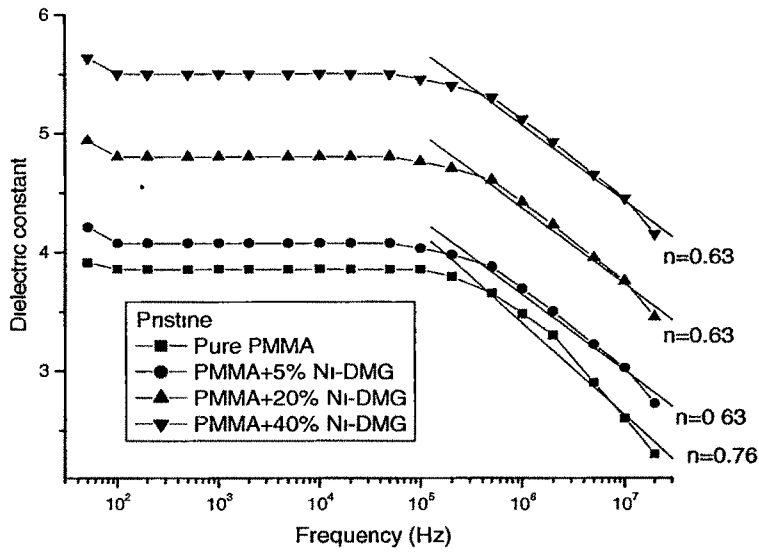


Figure 4.2(a) Dielectric constant versus frequency for pristine pure dispersed Ni-DMG in PMMA films.

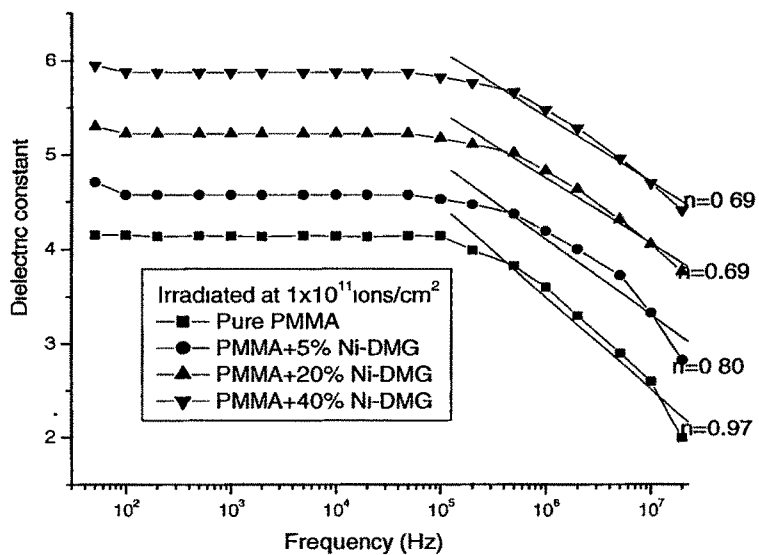


Figure 4.2(b) Dielectric constant versus frequency for irradiated (at the fluence of 1×10^{11} ions/cm²) pure and dispersed Ni-DMG in PMMA films.

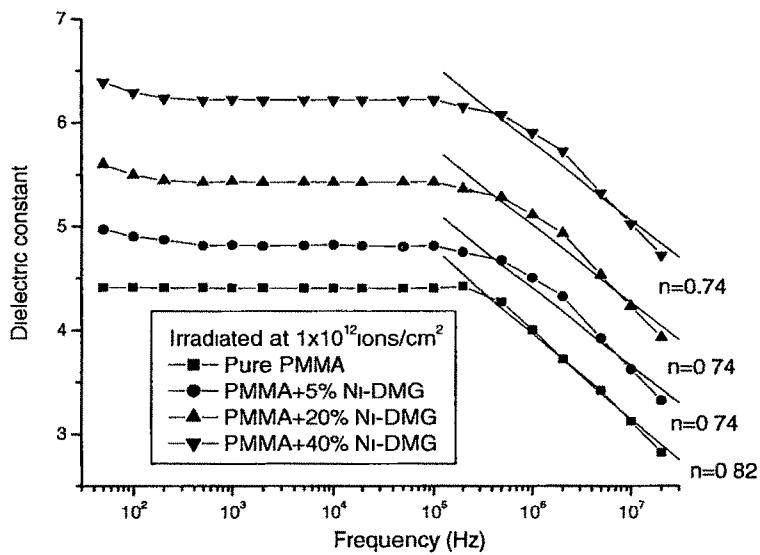
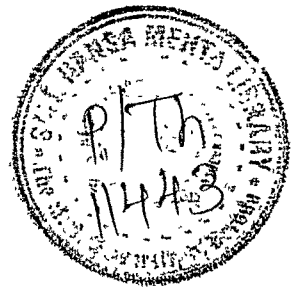


Figure 4.2(c) Dielectric constant versus frequency for irradiated (at the fluence of 1×10^{12} ions/cm²) pure and dispersed Ni-DMG in PMMA films.

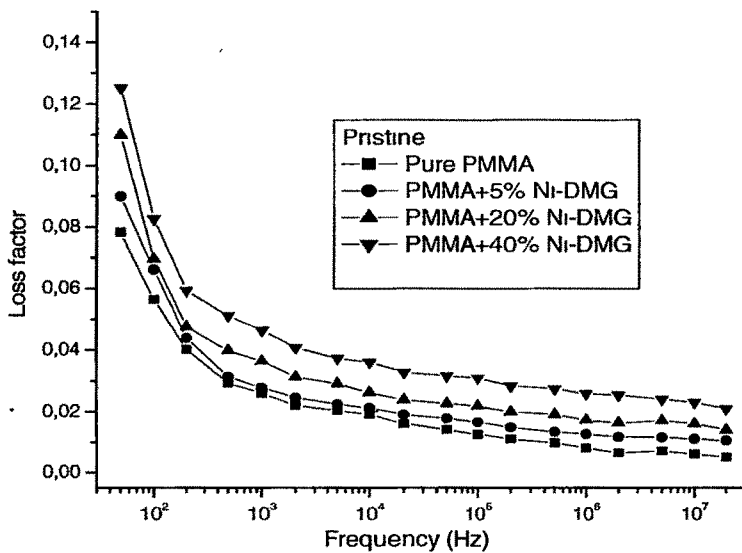


Figure 4.3 (a) Dielectric loss versus frequency for pristine pure and dispersed Ni-DMG in PMMA films.

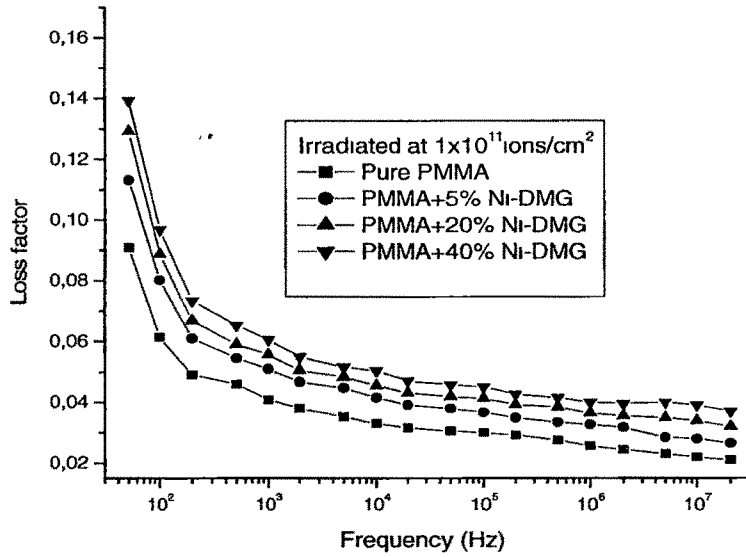


Figure 4.3 (b) Dielectric loss versus frequency for irradiated (at the fluence of 1×10^{11} ions/cm²) pure and dispersed Ni-DMG in PMMA films.

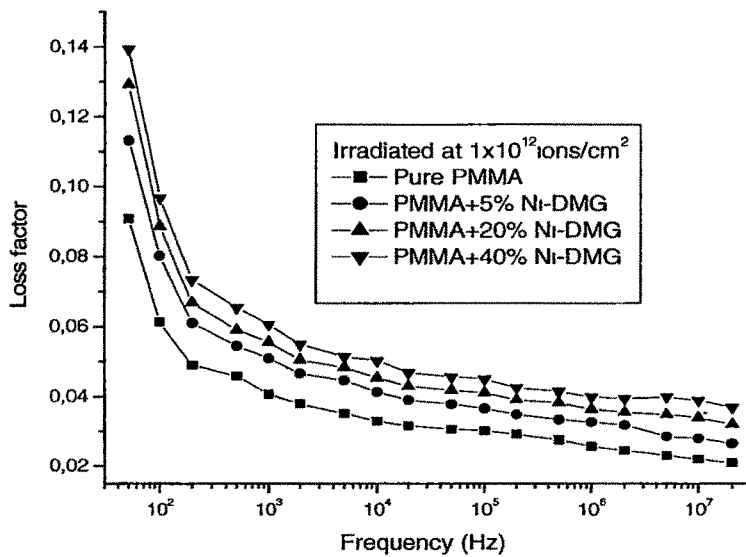


Figure 4.3 (c) Dielectric loss versus frequency for irradiated (at the fluence of 1×10^{12} ions/cm²) pure and dispersed Ni-DMG in PMMA films.

4.1.2 Microhardness

The Vicker's microhardness of all samples have been studied in the load range 25 mN to 1000 mN, and calculated by using the formula 2.10 as discussed in article 2.4.2 of Chapter 2. Fig.4.4(a, b and c) shows the plots of the Vickers' microhardness (H_v) versus applied load (P) for pristine and irradiated films of pure PMMA, and dispersed Ni-DMG compound of 5%, 20% and 40% in PMMA. It is observed that hardness (H_v) value increases with the loads upto 100 mN and then decreases and become saturated beyond the load of 400 mN.

The increase in hardness with load can be explained on the basis of strain hardening phenomenon. Beyond certain load, the polymer exhausts its strain hardening capacity and hardness tends to become constant. The rate of strain hardening is greater at low loads and decreases at higher loads. The value obtained from saturation region, therefore represents the true hardness of the bulk materials, since at high loads the indenter penetration depth is also high and surface effects become insignificant. It is also observed that hardness increases as fluence increases. This may be attributed to cross linking effect due to emission of hydrogen and/or other volatiles gases. The hydrogen depleted carbon network make the polymer harder [19, 20, 21].

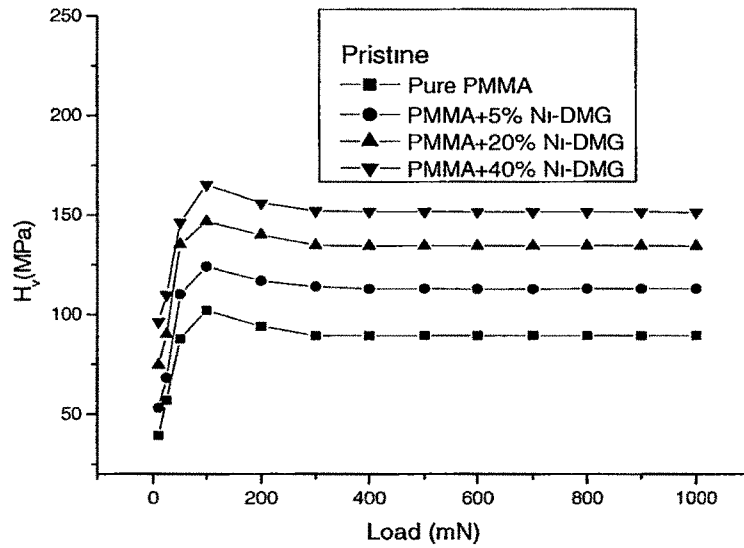


Figure 4.4(a) Plot of hardness (H_v) versus applied load (P) for pristine pure and dispersed Ni-DMG compound in PMMA films.

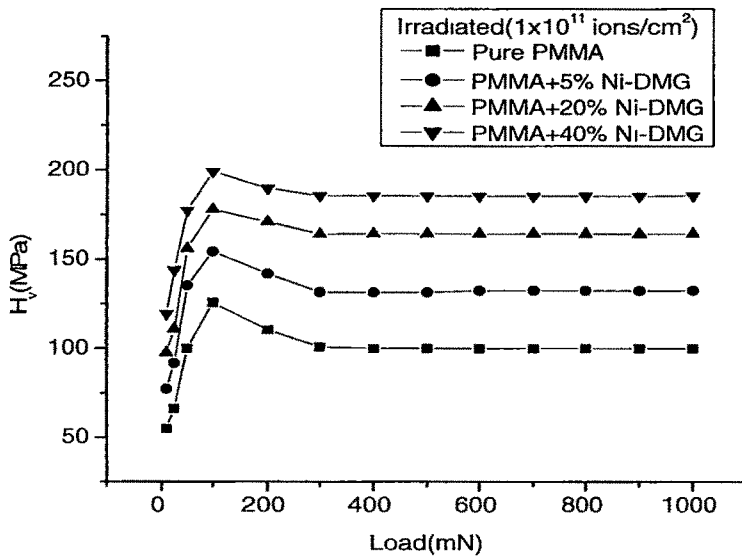


Figure 4.4(b) Plot of hardness (H_v) versus applied load (P) for irradiated (at the fluence of 1×10^{11} ions/cm²) pure and dispersed Ni-DMG compound in PMMA films.

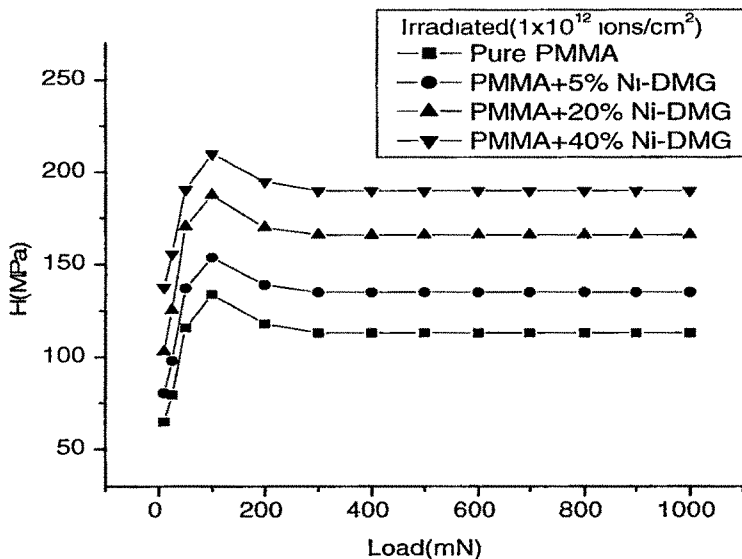


Figure 4.4 (c) Plot of hardness (H_v) versus applied load (P) for irradiated (at the fluence of 1×10^{12} ions/cm²) pure and dispersed Ni-DMG compound in PMMA films.

4.1.3 X-Ray Diffraction Studies

The changes in the crystallinity of pure PMMA and Ni-DMG compound dispersed at different concentrations of 5%, 20% and 40% in PMMA films due to high energy ion beam irradiation were investigated by X-ray diffraction. Fig. 4.5 shows X-ray diffractograms for Ni-DMG compound sample, this structure was earlier reported by L. Edward et al [22]. The average crystallite size of Ni-DMG compound corresponding to main peaks is 332.141 \AA as shown in Table 4.1. Fig. 4.6(a,b,c), 4.7(a,b,c), 4.8(a,b,c) and 4.9(a,b,c) show X-ray diffractograms for pure PMMA, 5%, 20% and 40% Ni-DMG

dispersed PMMA films respectively for pristine and irradiated samples at the fluences of 1×10^{11} , and 1×10^{12} ions/cm².

The main peak is observed in the case of pure PMMA (Fig 4.6) at $2\theta=13.1$, and intensity of this peak decreases on irradiation. It reveals the increase in the amount of amorphous content of PMMA. The crystallite size of Ni-DMG compound dispersed at different concentration (5%, 20% and 40%) in PMMA films before and after irradiation was calculated using Scherrer's equation 2.13 as discussed in article 2.45 of Chapter 2[23].

$$b=K \lambda/L \cos\theta \quad (4.1)$$

where b is full width at half maximum (FWHM) in radians, λ is the wavelength of X-ray beam (1.5418 \AA) and K , a constant (~ 0.9). The crystallite size, 2θ and b values are listed in Table 4.2, 4.3 and 4.4 for pristine 5% Ni-DMG, pristine 20% Ni-DMG and pristine 40% Ni-DMG dispersed PMMA films respectively. The average crystallite size is found 223.167 \AA , 346.342 \AA and 374.479 \AA respectively (Fig. 4.7,4.8 and 4.9) It reveals that the crystallite size increases on increasing the concentration, which may be attributed to increase in the density of particles with the increase in concentration of dispersed concentration of Ni-DMG compound in the polymer films. At the fluence of 1×10^{11} and 1×10^{12} ions/cm², the average crystallite size is found 205.987 \AA and 168.754 \AA for 5%, 335.624 \AA , 322.107 \AA for 20%, and 347.207 \AA and 347.588 \AA for 40% respectively. It is observed that the crystallite size decreases with increasing ion fluence [Table 4.2-4.4]. It reveals that irradiation leads to a narrow size distribution of particles by allowing minimum-sized nanoparticles to melt and fast quenching results in average sized particles in the sample. With the increase of ion fluence, average diameter increases until complete amorphization of the polymer. The particles become free standing, and under heavy dose,

some of them coalesce into bigger-sized grains and some split into smaller grains, the nature of coalescence or splitting solely depends upon the relative positions of the grains with respect to the point of ion impact [24]. In our case ion irradiation indicates that size distribution of Ni-DMG particles is narrow due to deposition of huge amount of energy and resulted splitting/melting of nanometric grain and amorphicity increases with the fluence due to bond breakage or chain scission. The average particle size of Ni-DMG dispersed PMMA at different concentration and at different fluences is summarised in Table 4.5.

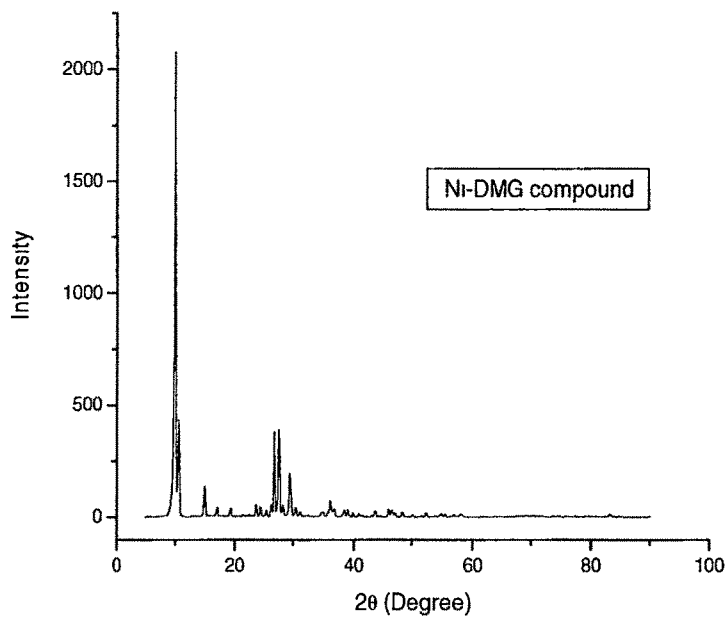


Figure 4.5 XRD diffraction pattern for Ni-DMG compound.

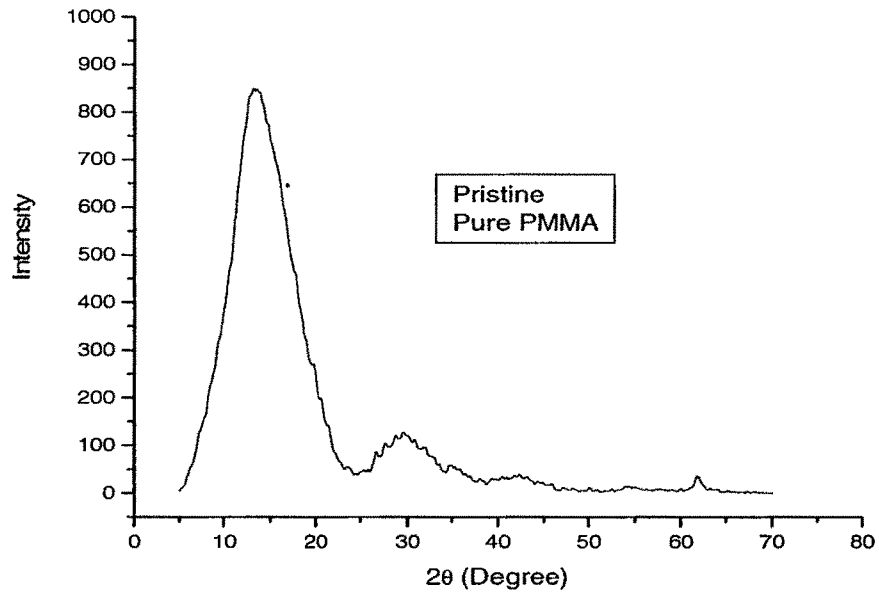


Figure 4.6 (a) XRD diffraction pattern for pure PMMA film (Pristine).

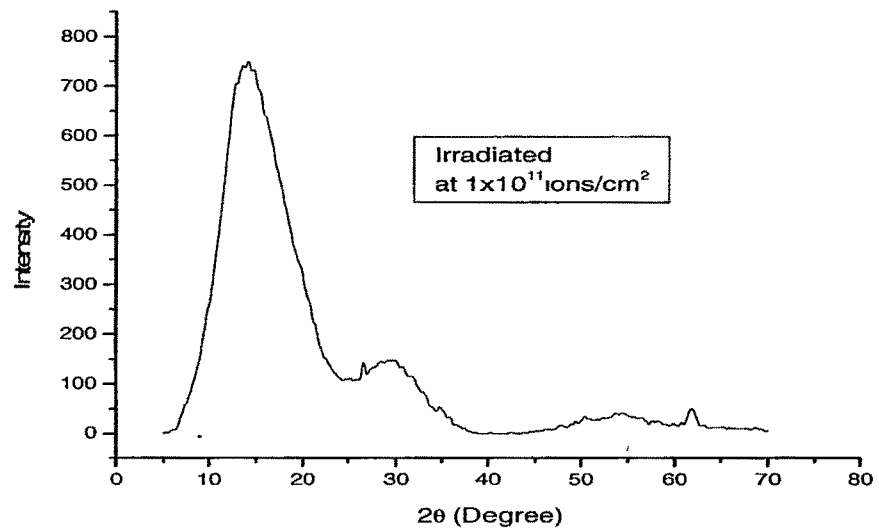


Figure 4.6(b) XRD diffraction pattern for pure PMMA film (at the fluence of 1×10^{11} ions/cm²).

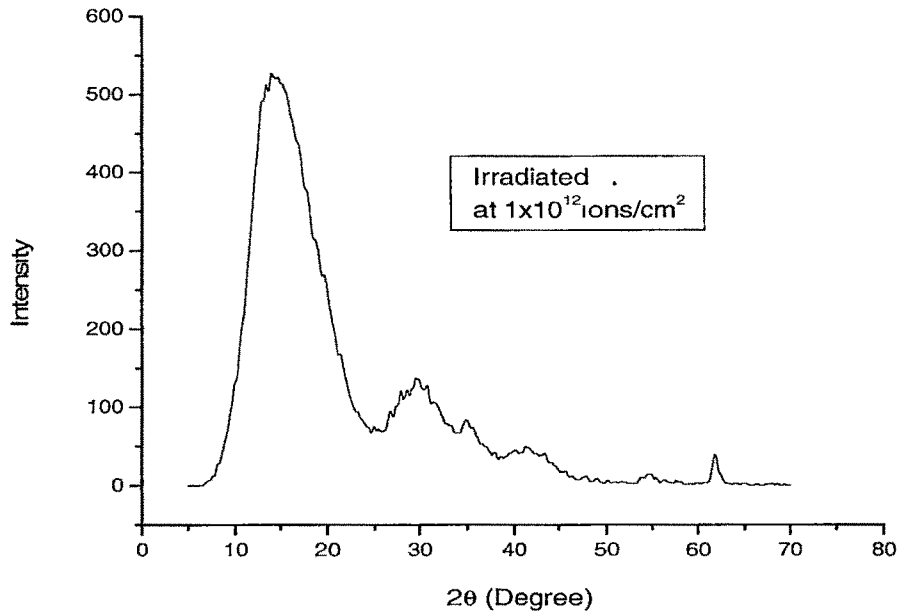


Figure 4.6(c) XRD diffraction pattern for pure PMMA film (at the fluence of 1×10^{12} ions/cm²).

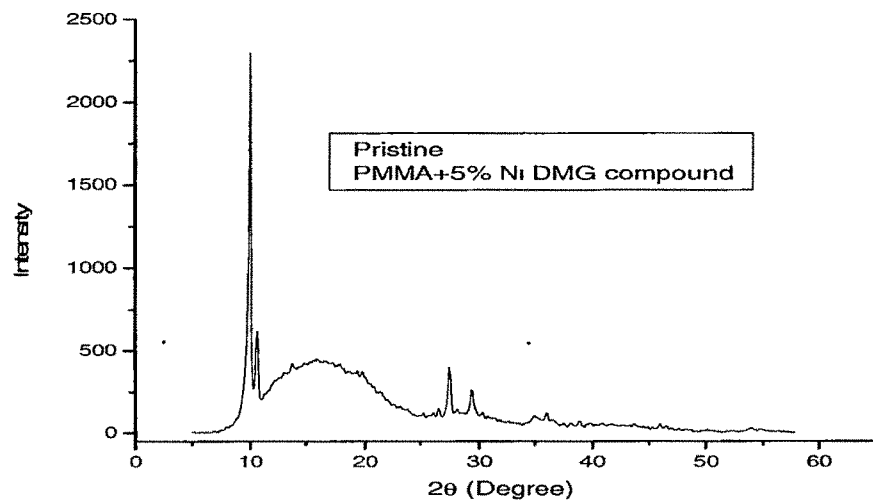


Figure 4.7(a) XRD diffraction pattern for 5% Ni- DMG compound dispersed in PMMA film (Pristine).

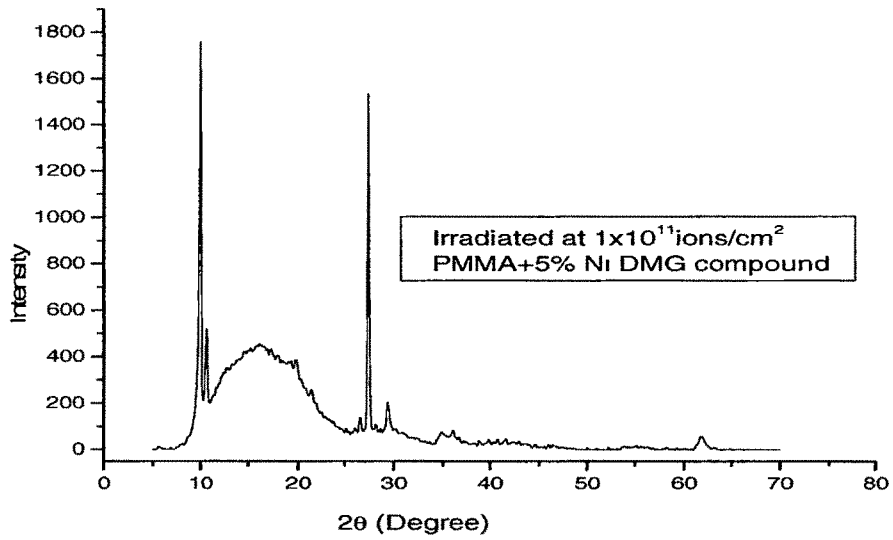


Figure 4.7(b) XRD diffraction pattern for 5% Ni- DMG compound dispersed in PMMA film for irradiated at the fluence of 1×10^{11} ions/cm².

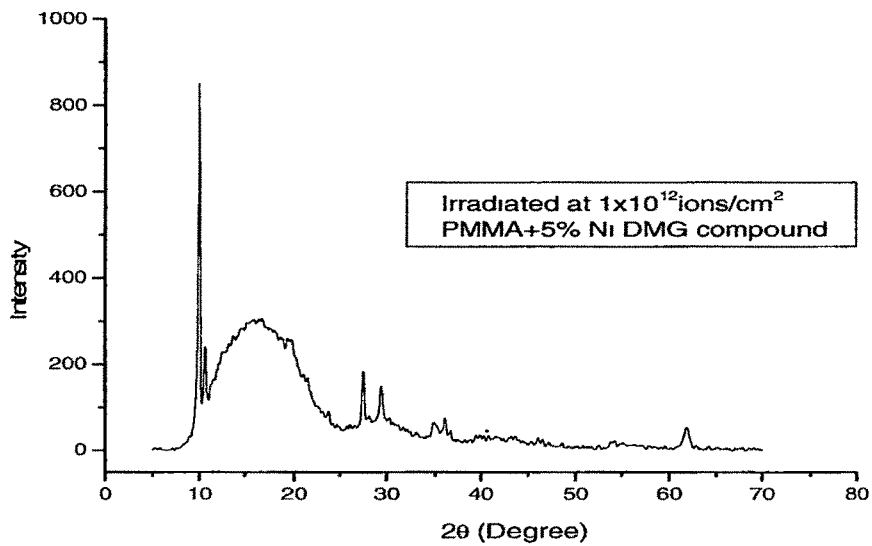


Figure 4.7(c) XRD diffraction pattern for 5% Ni- DMG compound dispersed in PMMA film for irradiated at the fluence of 1×10^{12} ions/cm².

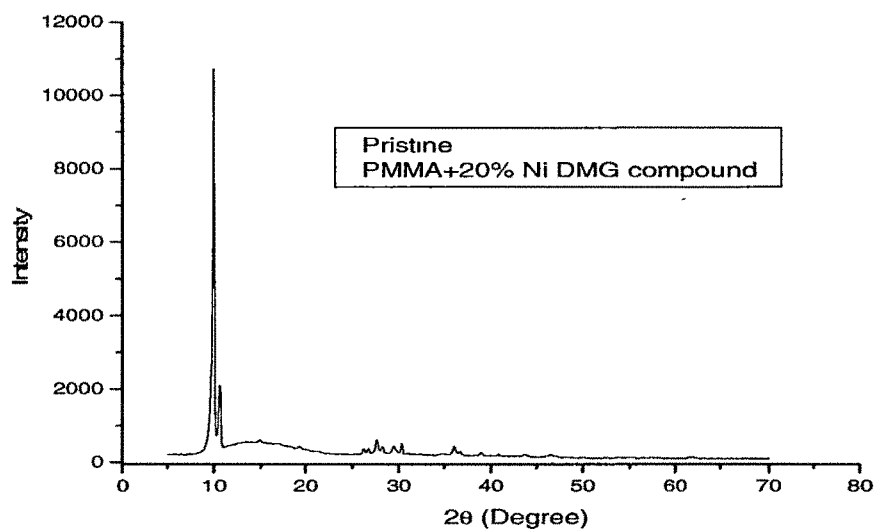


Figure 4.8(a) XRD diffraction pattern for 20% Ni- DMG compound dispersed in PMMA film (Pristine).

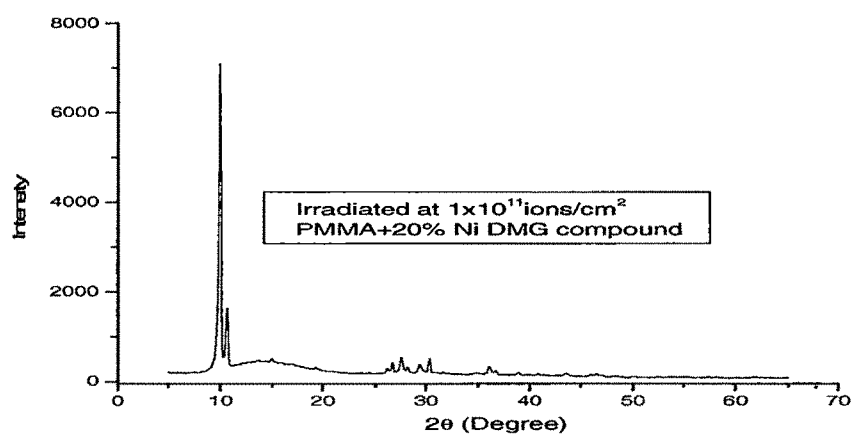


Figure 4.8(b) XRD diffraction pattern for 20% Ni- DMG compound dispersed in PMMA film for irradiated at the fluence of 1×10^{11} ions/cm².

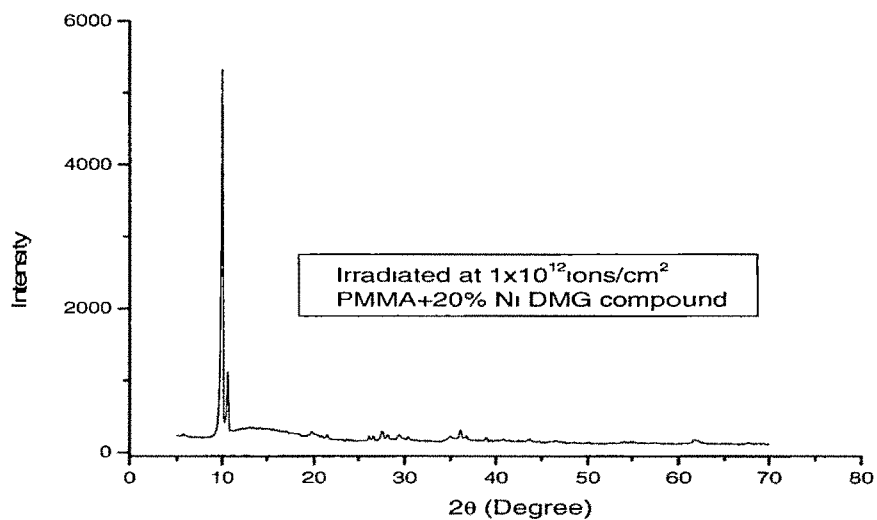


Figure 4.8(c) XRD diffraction pattern for 20% Ni- DMG compound dispersed in PMMA film for irradiated at the fluence of 1×10^{12} ions/cm².

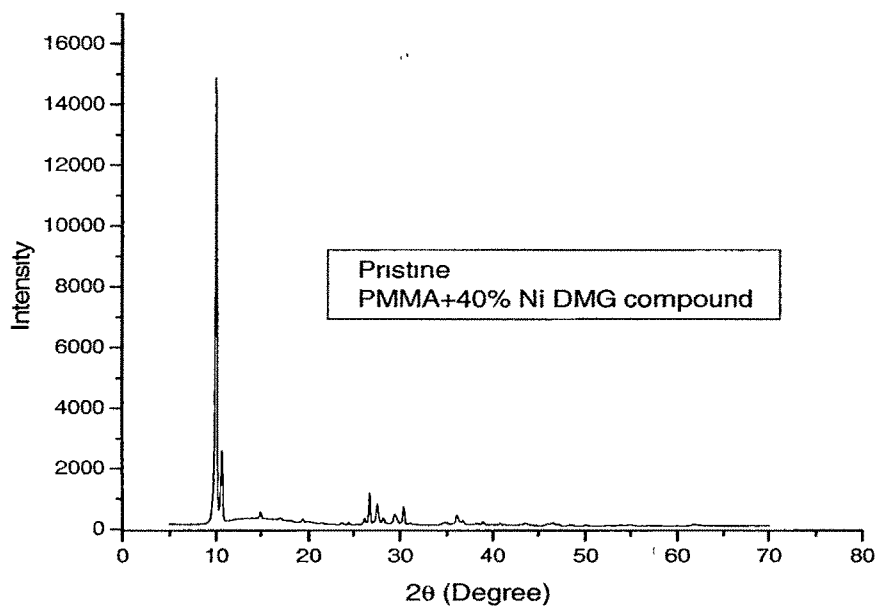


Figure 4.9(a) XRD diffraction pattern for 40% Ni- DMG compound dispersed in PMMA film (Pristine).

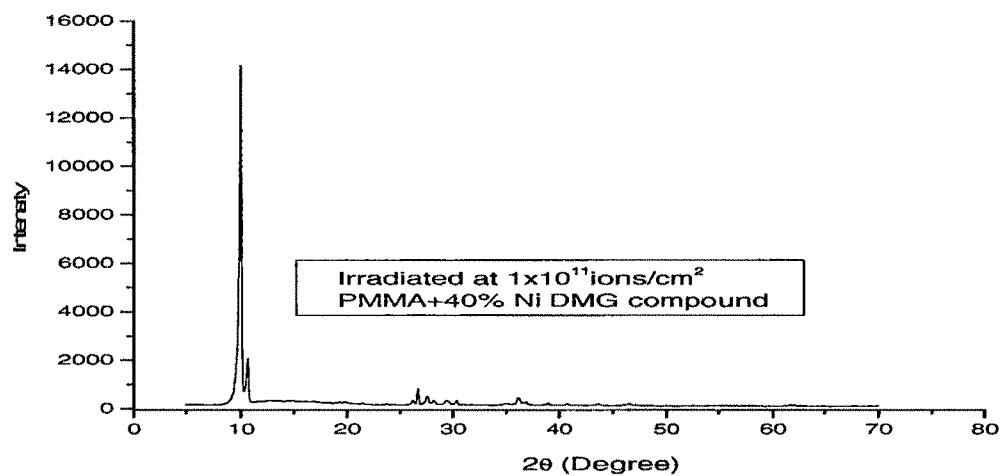


Figure 4.9 (b) XRD diffraction pattern for 40% Ni- DMG compound dispersed in PMMA films for irradiated at the fluence of 1×10^{11} ions/cm².

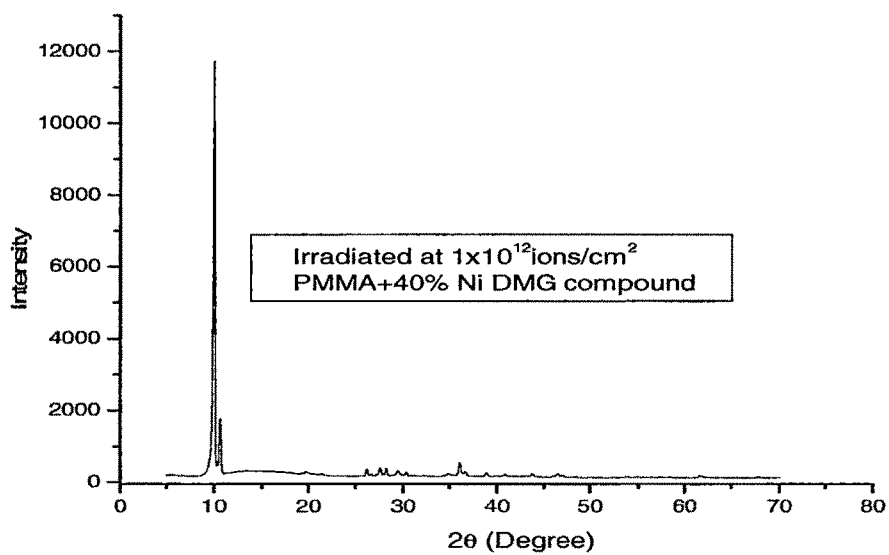


Figure 4.9(c) XRD diffraction pattern for 40% Ni- DMG compound dispersed in PMMA film for irradiated at the fluence of 1×10^{12} ions/cm².

Table-4.1: XRD parameters for Ni-DMG compound.

Ni-DMG compound			
2θ ($^{\circ}$)	FWHM b ($^{\circ}$)	$b\cos\theta$	Crystallite size (\AA)
10.005	0.1910	0.0033	417.722
10.642	0.2330	0.0040	342.600
24.361	0.2322	0.0039	350.179
26.791	0.3295	0.0055	249.409
26.711	0.2066	0.0035	395.403
29.387	0.2749	0.0046	298.905
36.067	0.3087	0.0051	270.771
Average crystallite size= 332.171 \AA			

Table-4.2: XRD parameters for pristine and irradiated 5% Ni-DMG compound dispersed PMMA films.

Pristine				at 1×10^{11} ions/cm ²				at 1×10^{12} ions/cm ²			
2θ (0)	FWHM b ($^{\circ}$)	$b\cos\theta$	Crystallite size (\AA)	2θ (0)	FWHM b ($^{\circ}$)	$b\cos\theta$	Crystallite size (\AA)	2θ (0)	FWHM b ($^{\circ}$)	$b\cos\theta$	Crystallite size (\AA)
10.000	0.2235	0.0038	359.115	9.997	0.2138	0.0037	373.173	9.994	0.2396	0.0041	332.989
10.628	0.3937	0.0068	202.753	10.631	0.3897	0.0067	204.835	27.561	0.3926	0.0066	208.448
29.382	0.7188	0.0121	114.311	26.629	1.8666	0.0316	43.756	29.416	1.000	0.0168	82.173
				27.454	0.1845	0.0031	443.458	36.067	1.8406	0.0305	45.404
				29.401	0.6060	0.0100	137.674				
				36.094	2.5306	0.0419	33.024				
Average crystallite size= 223.167 \AA				Average crystallite size= 205.987 \AA				Average crystallite size= 205.987 \AA			

Table-4.3: XRD parameters for pristine and irradiated 20% Ni-DMG compound dispersed PMMA films.

Pristine				at 1×10^{11} ions/cm ²				at 1×10^{12} ions/cm ²			
2 θ (°)	FWHM b (°)	bcos θ	Crystallite size (Å ⁰)	2 θ (°)	FWHM b (°)	bcos θ	Crystallite size (Å ⁰)	2 θ (°)	FWHM b (°)	bcos θ	Crystallite size (Å ⁰)
9.999	0.1833	0.0031	435.268	10.005	0.1999	0.0034	399.124	9.996	0.1977	0.0034	403.563
10.639	0.3101	0.0053	257.416	10.638	0.2931	0.0050	272.346	10.632	0.3317	0.0057	240.652
Average crystallite size= 346.342 Å ⁰				Average crystallite size= 335.624 Å ⁰				Average crystallite size= 322.107 Å ⁰			

Table-4.4: XRD parameters for pristine and irradiated 40% Ni-DMG compound dispersed PMMA films.

Pristine				at 1×10^{11} ions/cm ²				at 1×10^{12} ions/cm ²			
2 θ (°)	FWHM b (°)	bcos θ	Crystallite size (Å ⁰)	2 θ (°)	FWHM b (°)	bcos θ	Crystallite size (Å ⁰)	2 θ (°)	FWHM b (°)	bcos θ	Crystallite size (Å ⁰)
10.006	0.1817	0.0031	439.078	10.002	0.1895	0.0032	421.028	10.010	0.1634	0.0028	488.282
10.640	0.2576	0.0044	309.879	10.638	0.2919	0.0050	273.466	10.641	0.2297	0.0039	347.518
Average crystallite size= 374.479 Å ⁰				Average crystallite size= 347.207 Å ⁰				Average crystallite size= 347.588 Å ⁰			

Table-4.5: Average particle size of pristine and irradiated samples.

Sample	Pristine	At 1×10^{11} ions/cm ²	At 1×10^{12} ions/cm ²
		Average crystallite size (A ⁰)	Average crystallite size (A ⁰)
PMMA+5% Ni-DMG dispersed film	223.167	205.987	205.987
PMMA+20% Ni-DMG dispersed film	346.342	335.624	322.107
PMMA+40% Ni-DMG dispersed film	374.479	347.207	347.588

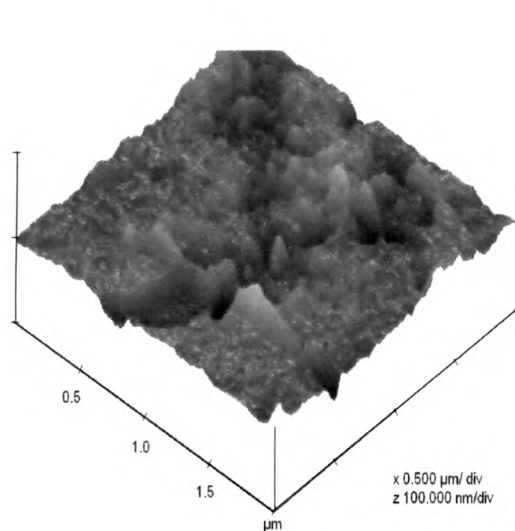
4.1.4 Surface Morphology

4.14 (a) Atomic Force Microscopy

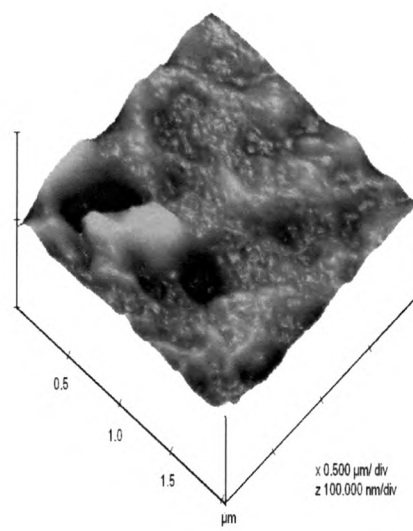
The surface morphology of pristine and irradiated films of pure PMMA, and 40% dispersed Ni-DMG PMMA was measured by AFM on $2 \times 2 \mu\text{m}^2$ area as shown in Fig 4.10. Each AFM image was analyzed in terms of surface average roughness (Ra). The average roughness values are 4.9 nm and 14 nm for unirradiated samples and those of irradiated samples the roughness values are 2 nm and 4.6 at the fluence of 1×10^{12} ions/cm².

It was found that roughness increases as Ni-DMG concentration increases. The increase in roughness may be due to the increase of density and size of metal particles on the surfaces of the PMMA films [25]. It is also observed that after irradiation the

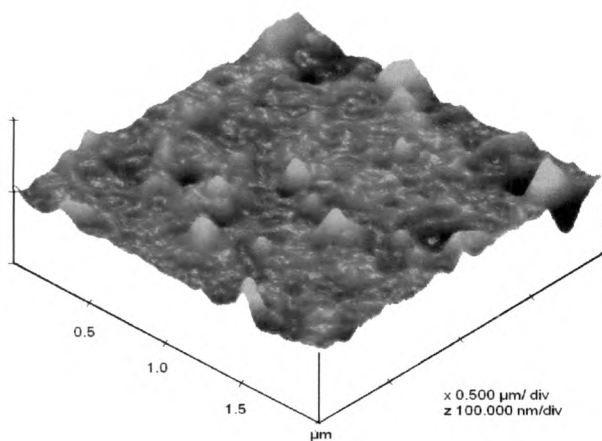
roughness of the surface decreases and the surface becomes significantly smoother. This relative smoothness is probably due to defect enhanced surface diffusion [26, 27].



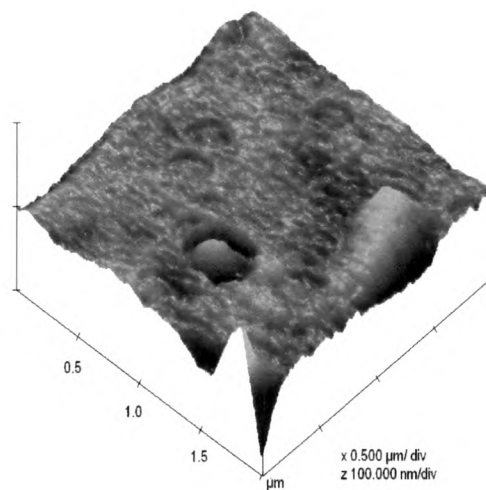
4.10(a)



4.10(b)



4.10(c)



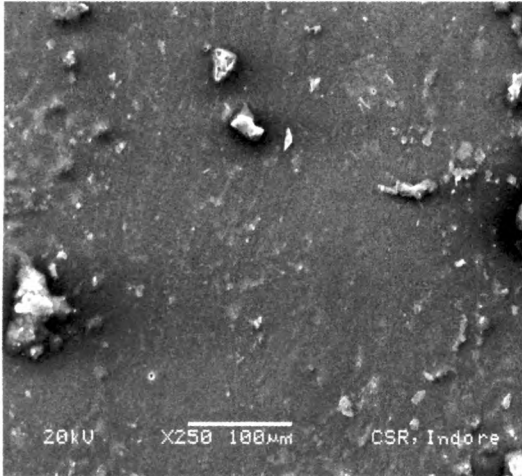
4.10(d)

Figure 4.10 (a) AFM image of pure PMMA film (pristine) (b) dispersed Ni-DMG (40%) in PMMA film (pristine) (c) pure PMMA film (irradiated at the fluence of 1 x

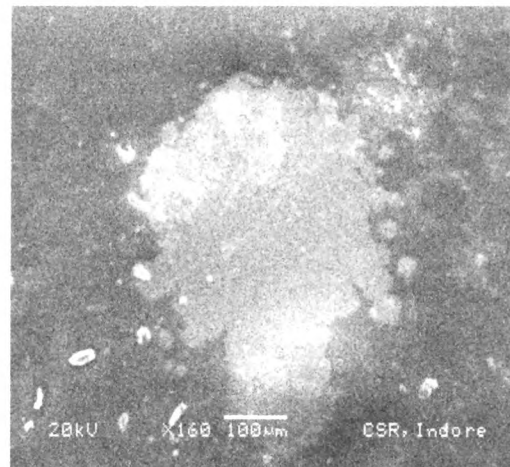
10^{12} ions/cm²) (d) dispersed Ni-DMG (40%) in PMMA film (irradiated at the fluence of 1×10^{12} ions/cm²).

4.1.4 (b) Scanning Electron Microscopy

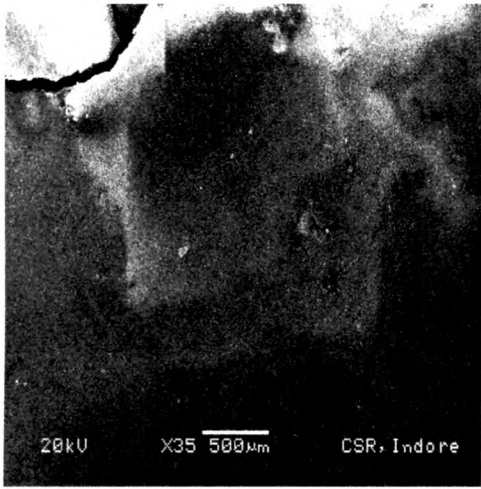
The surface morphology studies of pure and Ni-DMG dispersed PMMA films were carried out by taking SEM images before and after irradiations. Fig.4.11 shows the surface morphology of pure PMMA, and dispersed Ni-DMG compound of 5% and 40% in PMMA films for pristine [Fig. 4.11 (a, b,c)] and irradiated samples at the fluences of 1×10^{11} ions/cm² [Fig. 4.11 (d,e,f)] and 1×10^{12} ions/cm² [Fig 4.11 (g,h,i)] respectively. After irradiation partial agglomeration of fillers and flake-like structures could be seen in the micrographs of SEM.



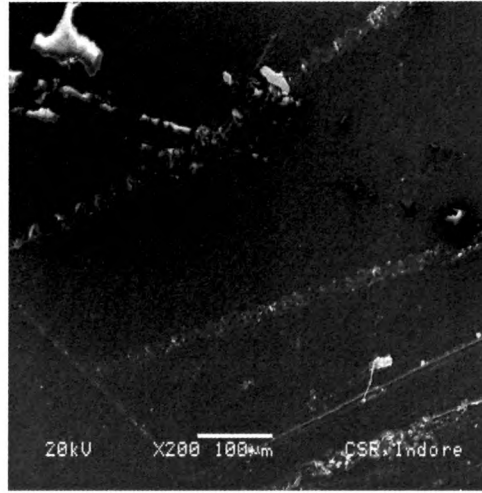
4.11(a)



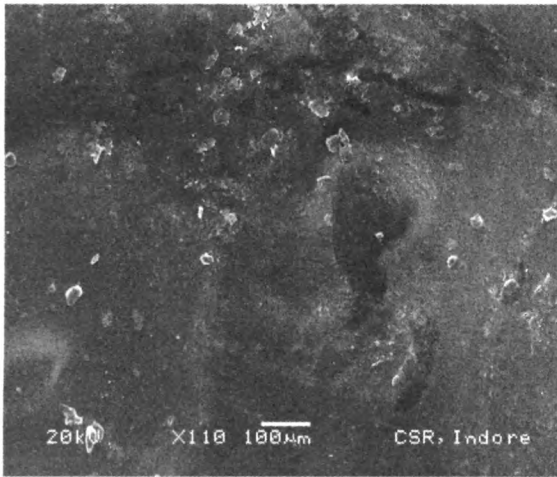
4.11(b)



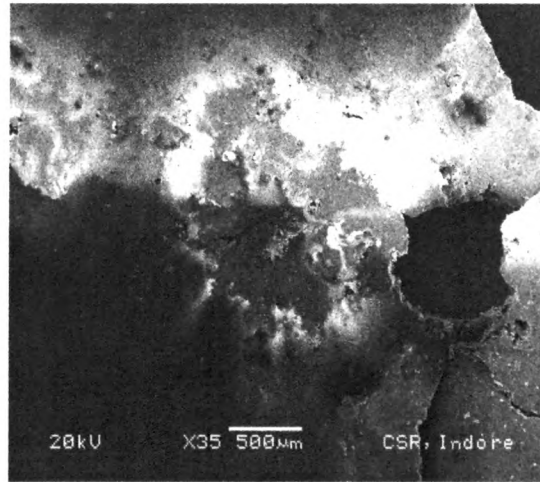
4.11(c)



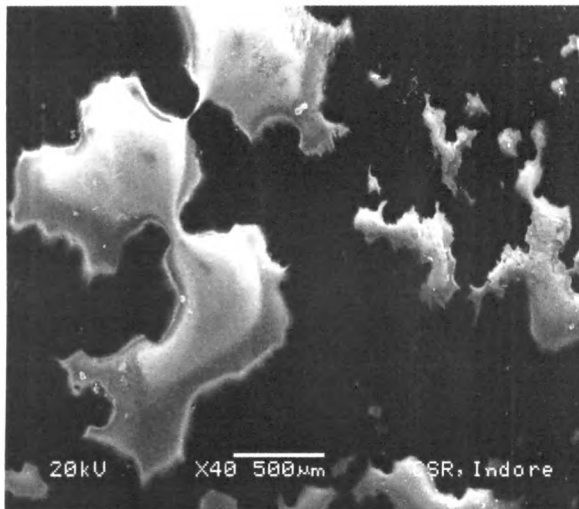
4.11(d)



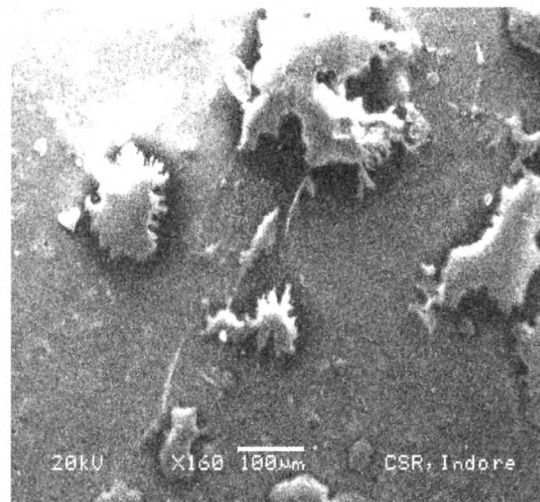
4.11(e)



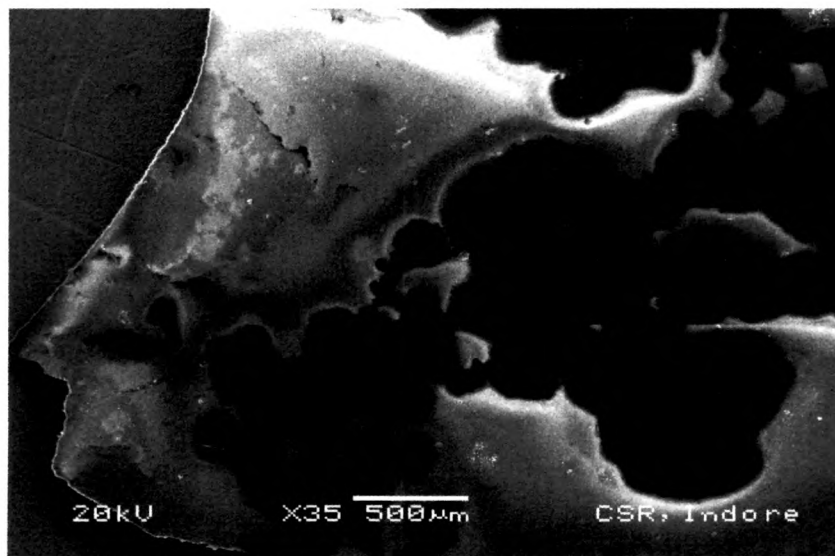
4.11(f)



4.11(g)



4.11(h)



4.11(i)

Figure 4.11(a) SEM micrograph of pure PMMA film (pristine) (b) dispersed Ni-DMG (5%) in PMMA film (pristine) (c) dispersed Ni-DMG (40%) in PMMA film (pristine) (d) pure PMMA film (irradiated at the fluence of 1×10^{11} ions/cm²) (e) dispersed Ni-DMG (5%) in PMMA film (irradiated at the fluence of 1×10^{11} ions/cm²)

(f) dispersed Ni-DMG (40%) in PMMA film (irradiated at the fluence of 1×10^{11} ions/cm²) (g) pure PMMA film (irradiated at the fluence of 1×10^{12} ions/cm²) (h) dispersed Ni-DMG (5%) in PMMA film (irradiated at the fluence of 1×10^{12} ions/cm²) (i) SEM micrgraph of dispersed Ni-DMG (40%) in PMMA film (irradiated at the fluence of 1×10^{12} ions/cm²).

4.2 Conclusion

The changes in the crystallinity of pure PMMA and Ni-DMG compound dispersed at different concentration of 5%, 20% and 40% in PMMA composite films were observed by X-ray diffraction due to high energy ion beam irradiation. It is observed that the crystallize size decrease with the fluence of ion beam. It reveals that irradiation leads to a narrow size distribution of particles by allowing minimum-sized nanoparticles to melt and fast quenching results in average sized particles in the sample. Ion irradiation indicates that size distribution of Ni-DMG particles is narrow due to deposition of huge (large) amount of energy and resulted in splitting/melting of nanometric grain. The amorphicity increases with the fluence due to chain scission of polymeric samples. It is observed that dielectric and microhardness of organometallic compound dispersed PMMA films is greatly enhanced by ion beam irradiation. It may be attributed to (i) metal to polymer bonding and (ii) conversion of the polymeric structure in to hydrogen depleted carbon network. Thus irradiation makes the polymer harder, more conductive. Dielectric loss and constant are observed to change significantly with the fluence. This might be attributed to breakage of chemical bonds and resulting in the increase of free radicals, unsaturation etc. It is also observed that dielectric constant obeys Universal law of dielectric response. Vickers'

microhardness studied reveals that microhardness of organometallic compound dispersed PMMA films enhanced significantly due to increase of concentration of Ni-DMG compound and also with the fluence. The surface roughness increases as Ni-DMG concentration increases and decreases on irradiation as observed from AFM studies. After irradiation partial agglomeration of fillers and flake-like structures were observed in the micrographs of SEM.

References

- [1] R.C.Gupta, D.C.Kothari, R.J.Choudhari, Ravi Kumar, P.K.Sahoo, K.P.Lieb, S.Klaumunzer, Nucl. Instr. and Meth. **B245** (2006) 219.
- [2] Y. Takeda, V. T. Gritsyna, N. Umeda, C. G. Lee, N. Kishimoto, Nucl. Instr. and Meth. **B 148** (1999) 1029.
- [3] S.O.Kucheyev, J.S.Williams, J.Zou, C.Jagadish, G.Li, Nucl. Instr. and Meth. **B178** (2001)209.
- [4] E.Valentin, H.Bernas, C.Ricolleau, F.Creuzet, Phys.Rev.Lett.**86** (2001) 99.
- [5] V.Naundorf, Int. J. Mod.Phys. **B6** 18(1992) 2925.
- [6] S. Heimer, Nature **408** (2000) 531.
- [7] R. L. Fleischer, P. B. Price, R. M. walker, Nuclear Tracks in Solids, University of California Press, Berkely, CA,1975.
- [8] A. Qureshi, N.L.Singh, S. Shah, F.Singh, and D.K.Avasthi, Communicated for the presentation in International conference on Ion Beam Analysis (IBA), 23rd Sept-26th Sept, 2007, Hyderabad.
- [9] Anjum Qureshi, N.L.Singh, Sejal Shah, F.Singh, D.K.Avasthi, Journal of Macromolecule Sci. (communicated).
- [10] M. Abu-Abdeen, GM. Nasr, H. M. Osman and A. I. Abound. Egypt. J. Sol. **25**, (2002) 275.
- [11] Ye. P. Mamunya, V. V. Davydenko, P. Pissis, E. V. Lebedev, European Polymer Journal **38** (2002)1887.
- [12] Y. Q. Wang, M. Curry, E. Tavenner, N. Dobson, R. E. Giedd. Nucl.Instr. & Meth. **B 219-220** (2004)798.

- [13] Psarras GC, Manolaki E, Tsangarris GM. *Composites A* 2001; 33:375.
- [14] Ghany AE, Salam AE, Nasr GM. *J Appl Polym Sci* 2000; 77:1816.
- [15] A. K. Jonscher. *Dielectric relaxation in solids*. London: Chesla dielectric press; 1983.
- [16] A. K. Jonscher, *Nature* **267** (1977) 673.
- [17] T.Phukan, D. Kanjilal, T. D. Goswami, H. L. Das, *Nucl Instr and Meth B***234** (2005) 520.
- [18] N. P. Bogoroditsky, V. V. Pasyukov, B. M. Tareev, *Electrical Engineering Materials*, Mir Publisher Moscow (1974).
- [19] N. L. Singh, A. Qureshi, F. Singh, D. K. Avasthi, *Mat. Sci. Eng. B* **137** (2007) 85.
- [20] S. K. Awasthi and Bajoai, *Indian Journal of Pure Applied Physics* **39** (2001)795.
- [21] E.H.Lee, G.R.Rao.L.K. Mansur, *Mater. Sci. Forum* **248-249** (1997) 135.
- [22] L. Edward Godycki and R. E. Rundle, *Acta Cryst.* **6** (1953) 487.
- [23] L. V. Azaroff, *Elements of X-ray crystallography*, McGraw Hill Book Co., USA, 1968.
- [24] D. Mohanta, N. C. Mishra, A. Choudhury, *Material Letters* **58** (2004) 3694.
- [25] Xingbin Yan, Tao Xu, Shan Xu, Xiaobo Wang and Shengrong Yang. *Nanotechnology* **15**(2004)1759.
- [26] Yatendra S. Chaudhary, Saif A. Khan, Rohit Shrivastava, Vibha R. Satsangi, Satya Prakash, Umesh K. Tiwari, D. K. Avasthi, Navendu Goswami, Sahab Dass, *Thin Solid Films* **492** (2005)332.

- [27] A. Biswas, D. K. Avasthi, D. Fink, J. Kanzow, U. Schurmann, S. J. Ding, O. C. Aktas, U. Saeed, V. Zaporozhchenko, F. Faupel, R. Gupta, N. Kumar, Nucl. Instr. and Meth **B 217** (2004) 29.